Numerical Simulations of Plasma Based Flow Control Applications

Y. B. Suzen[*], P. G. Huang[†], J. D. Jacob[‡]
Department of Mechanical Engineering, University of Kentucky, Lexington, KY 40506

and

D. E. Ashpis[§]
NASA John H. Glenn Research Center at Lewis Field, Cleveland, OH 44135

A mathematical model was developed to simulate flow control applications using plasma actuators. The effects of the plasma actuators on the external flow are incorporated into Navier Stokes computations as a body force vector. In order to compute this body force vector, the model solves two additional equations: one for the electric field due to the applied AC voltage at the electrodes and the other for the charge density representing the ionized air. The model is calibrated against an experiment having plasma-driven flow in a quiescent environment and is then applied to simulate a low pressure turbine flow with large flow separation. The effects of the plasma actuator on control of flow separation are demonstrated numerically.

Nomenclature

C_p	=	pressure coefficient
C_x	=	axial chord for Pak-B blade
e	=	elementary charge, C
$\vec{E}$	=	electric field, N/C
ε	=	permittivity, $\varepsilon = \varepsilon_r \varepsilon_o$
ε_r	=	relative permittivity
ε_o	=	permittivity of free space, 8.854×10^{-12} C^2/Nm^2
$\vec{f}_B$	=	body force vector, N/m^3
FSTI	=	freestream turbulence intensity, %
Φ	=	total electric potential, Volt, $\Phi = \phi + \varphi$
ϕ	=	electric potential due to external electric field, Volt
φ	=	electric potential due to net charge density, Volt
k	=	Boltzmann's constant
L_e	=	length of the electrode
λ_d	=	Debye length, m
μ	=	location parameter for Gaussian distribution
n_i	=	ion density in the plasma

[*]Sr. Engineer Associate, Department of Mechanical Engineering, 216A RGAN Bldg., suzen@engr.uky.edu, Member AIAA.
[†]Professor and Director of Graduate Studies, Department of Mechanical Engineering, 151 RGAN Bldg., ghuang@engr.uky.edu, Senior Member AIAA.
[‡]Associate Professor, Department of Mechanical Engineering, 151 RGAN Bldg., Senior Member AIAA.
[§]Aerospace Engineer, Turbine Branch, MS 5-11, 21000 Brookpark Road, Senior Member AIAA.

n_e	=	electron density in the plasma
n_o	=	background plasma density
ω	=	frequency, Hz
Re	=	Reynolds number based on inlet velocity and axial chord
ρ_c	=	net charge density, C/m^3
σ	=	scale parameter for Gaussian distribution
t	=	time, s
T	=	temperature of the species
U_{in}	=	inlet velocity
U	=	streamwise velocity
x, y	=	coordinates
y_n	=	wall normal distance

I. Introduction

Recent advances in the area of flow control have led to the application of new flow control strategies to various flow fields.[1-3] One of the major areas for applications of flow control is the gas turbine, which has the potential to lead to significant benefits in improved design and performance.[4,5] Several researchers have investigated the effectiveness and feasibility of different flow control methods for reducing losses and improving performance in gas turbine engine component flowfields.[6-9] Although many of these flow control methods have been beneficial in laboratory tests, the incorporation of such systems into actual applications is not straightforward. It involves development and testing of the control system for the actuators, as well as the hardware development of the device. An experimental approach requires numerous costly and time consuming trial-and-error iterations. With advances in computational fluid dynamics (CFD) and computer hardware, CFD offers an alternative method for designing and understanding complicated flow control systems. Continued development of CFD simulation tools and control algorithms is essential in order to adapt the available flow control technologies to design of modern gas turbine engines.

Among the active flow control techniques the use of plasma actuators has been demonstrated to be effective in several applications including flow separation and boundary layer control. The plasma actuators consist of two electrodes that are located on surface separated by a dielectric material as shown in Fig. 1. A high-voltage AC supplied to the electrodes causes the air in their vicinity to weakly ionize. The ionized air (plasma) in the presence of the electric field gradient produced by the electrodes, result in a body force vector acting on the external flow that can induce steady or unsteady velocity components. The effectiveness of plasma actuators in controlling flow separation has been demonstrated by several researchers. Examples of various applications include boundary layer control by Roth et al.[10], exciting boundary layer instabilities on a sharp cone at Mach 3.5 by Corke et al.[11], lift augmentation

Figure 1. Schematic of plasma actuator.

on a wing section by Corke et al.[12], wing section leading edge separation control by Post and Corke[13], unsteady vortex generation by Orlov et al.[14], separation control on low pressure turbine blades by Hultgren and Ashpis[15], Huang et al.[9] and Jacob et al.[16], separation control on stationary and oscillating airfoils by Post and Corke[17], and tip clearance control in turbines.[18] The results from these experiments indicate that several parameters have to be taken into consideration for effective flow control. The important parameters are location of the actuators on the surface, orientation, size, and relative placement of the embedded and exposed electrodes, applied voltage, and frequency of the actuation. The many parameters affecting the performance of the actuators makes incorporation of such systems into actual applications and the development and testing of optimized control systems for actuators a complicated task. CFD simulation tools can enable design and optimization of such complex flow control systems.
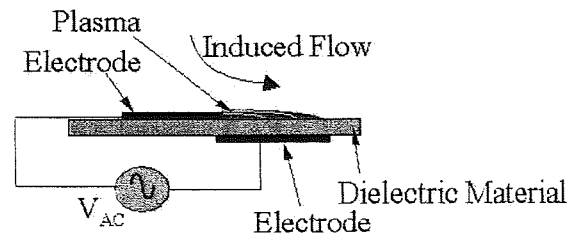
Computational studies of plasma flow control have been limited in comparison to the vast number of experimental studies. Examples of computational work include modeling of the effects of the plasma actuator on the external flow as a time averaged mean body force distribution in a triangular area located above the embedded electrode by Shyy et al.[19], modeling the effects of plasma actuators using a potential flow method based on a doublet model by Hall et al.[20], and simulation of plasma actuator effects using a lumped parameter model by Orlov and Corke[21]. In contrast to these simpler approaches, Roy and Gaitonde[22,23] modeled the collisional surface dielectric barrier discharge at atmospheric pressures by solving the charge continuity, charge momentum, electric field and potential distribution. In their approach helium was used as the carrier gas because its plasma coefficients and chemistry were available and the electric force obtained as a product of the charge and electric field was used to calculate the flow actuation effect.

In this paper, we outline a new numerical simulation methodology for active flow separation control applications using plasma actuators. This is computationally efficient and easy to implement into existing RANS codes. In this new approach, the effect of the plasma actuators on the external flow is incorporated into Navier Stokes computations as a body force vector. The body force is obtained as a product of the net charge density and the electric field. The new model solves the Maxwell equation to obtain the electric field due to the applied AC voltage at the electrodes and an additional equation for the charge density representing the plasma density. Details of the model development and implementation are provided below. Results of computations for a single plasma actuator in quiescent flow and computations of flow separation control over a Pak-B low-pressure turbine blade using a single plasma actuator are given in section 3. Concluding remarks are provided in section 4.

II. Plasma Physics Modeling and CFD Computations

The plasma actuators are formed by a pair of electrodes separated by a dielectric material. The actuator is placed in the surface with one electrode exposed to the surroundings and the other one embedded in the surface below the dielectric material (Figure 1). When a high-voltage AC is supplied to the electrodes, this arrangement causes the air in their vicinity to weakly ionize. The ionized air in the presence of the electric field gradient produced by the electrodes, results in a body force vector acting on the external flow that can induce steady or unsteady velocity components. This body force can be expressed in terms of the applied voltage and incorporated into the Navier Stokes equations. By neglecting magnetic forces, the electrohydrodynamic (EHD) force can be expressed as

$$\vec{f}_B = \rho_c \vec{E} \tag{1}$$

where, $\vec{f}_B$ is the body force per unit volume, ρ_c is net the charge density and $\vec{E}$ is the electric field. If the time variation of the magnetic field is negligible, as is often the case in plasma, the Maxwell's equations give rise to $\nabla \times E \approx 0$. This implies that the electric field can be derived from the gradient of a scalar potential[10,24]:

$$\vec{E} = -\nabla\Phi. \tag{2}$$

Gauss's law yields:

$$\nabla \cdot (\varepsilon \vec{E}) = \rho_c \tag{3}$$

or

$$\nabla \cdot (\varepsilon \nabla \Phi) = -\rho_c \tag{4}$$

where ε is the permittivity. The permittivity can be expressed as:

$$\varepsilon = \varepsilon_r \varepsilon_o \tag{5}$$

where ε_r is the relative permittivity of the medium, and ε_o is the permittivity of free space.

There still remains some controversy as to the physical mechanism by which the plasma actuator modifies the surrounding flow field. While it is clear that the body force developed via equation (1) has a large impact on the flow field, there is still some debate as to the effect of local temperature rise and reduced viscosity on the boundary layer. This accounts for the increase in velocity in the plasma region by increasing the shear rate to keep the viscous stress constant, as suggested by Leonov et al.[25]. Recent measurements appear to discount this reasoning, due to the large impact the small plasma region has on the surrounding flow[16]. Instead, the plasma region acts much like a source term in this regard.

Since the gas particles are weakly ionized, we can assume the potential Φ can be decoupled into two parts: one being a potential due to the external electric field, ϕ, and the other being a potential due to the net charge density in the plasma, φ,

$$\Phi = \phi + \varphi. \tag{6}$$

This approach is similar to the one used in numerical simulation of electroosmotic flows in which case the external electric field generates a force on the charged particles creating flow[26].

If we assume that the Debye thickness is small and the charge on the wall is not large, the distribution of charged species in the domain is governed by the potential on the wall due to the electric charge on the wall and is affected very little by the external electric field. Therefore, we can write two separate equations in terms of these two potentials, one for the external electric field due to the applied voltage at the electrodes:

$$\nabla \cdot (\varepsilon_r \nabla \phi) = 0 \tag{7}$$

and another one for the potential due to the charged particles:

$$\nabla \cdot (\varepsilon_r \nabla \varphi) = -(\rho_c / \varepsilon_o). \tag{8}$$

Equation (7) is solved for the electric potential, ϕ, using the applied voltage on the electrodes as boundary conditions. The boundary conditions and the computational domain for Equation (7) are shown in Figure 2 for a single pair of electrodes. Equation (7) is solved with the appropriate ε_r value on both the air side and the wall. For air, $\varepsilon_r = 1.0$. We chose Kapton as the dielectric material, as in the experiments and it has an ε_r value of 2.7. On the wall-air interface
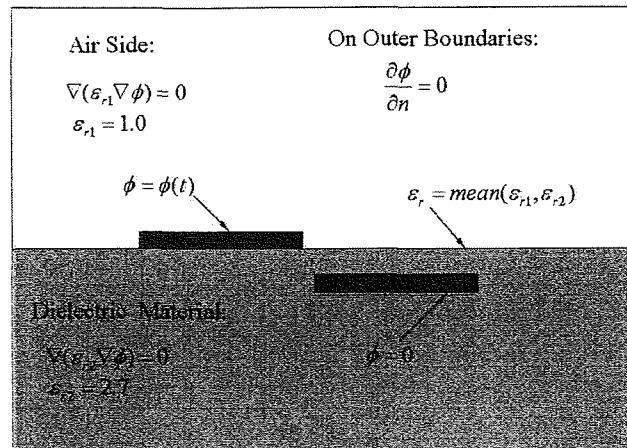

Figure 2. Computational domain and boundary conditions for Equation 7.

harmonic mean of ε_{r1} and ε_{r2} must be used in order to conserve electric field as shown in Figure 3. In this figure point 1 is on air side and point 2 is in the dielectric material, with point f on the interface.
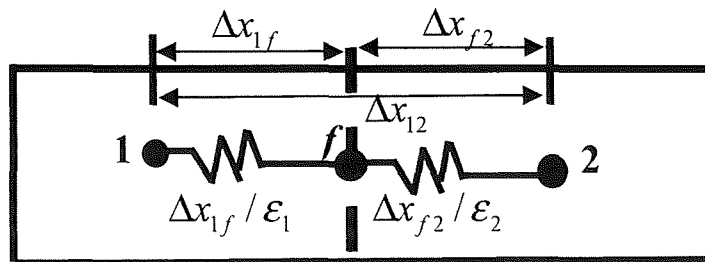

Figure 3. The interfacial permittivity.

At the dielectric wall and air interface, the electric field is conserved as shown in figure 3 by writing:

$$-\varepsilon_r \left(\frac{\partial \phi}{\partial x} \right)_f = -\varepsilon_1 \left(\frac{\partial \phi}{\partial x} \right)_{1 \to f} = -\varepsilon_2 \left(\frac{\partial \phi}{\partial x} \right)_{f \to 2} \tag{9}$$

or:

$$\frac{\phi_1 - \phi_2}{\left(\Delta x_{12}\middle/\varepsilon_f\right)} = \frac{\phi_1 - \phi_f}{\left(\Delta x_{1f}\middle/\varepsilon_1\right)} = \frac{\phi_f - \phi_2}{\left(\Delta x_{f2}\middle/\varepsilon_2\right)}. \tag{10}$$

By using the electric analogy as shown in figure 3, the interfacial permittivity, ε_f, should take the harmonic mean of the permittivity of air, ε_1, and the permittivity of dielectric material, ε_2:

$$\varepsilon_f = \frac{\varepsilon_1 \varepsilon_2}{\varepsilon_1 \dfrac{\Delta x_{f2}}{\Delta x_{12}} + \varepsilon_2 \dfrac{\Delta x_{1f}}{\Delta x_{12}}}. \tag{11}$$

Applied AC voltage imposed at the exposed (upper) electrode as boundary condition is:

$$\phi(t) = \phi^{\max} f(t) \tag{12}$$

The wave form function, $f(t)$, can be a sine wave given by:

$$f(t) = \sin(2\pi\omega t) \tag{13a}$$

or it can be a square wave given by:

$$f(t) = \begin{cases} 1 & \text{for } \sin(2\pi\omega t) \geq 0 \\ -1 & \text{for } \sin(2\pi\omega t) < 0 \end{cases} \tag{13b}$$

where ω is the frequency and $\phi^{\max}$ is the amplitude. The embedded electrode is prescribed as ground by setting the electric potential to zero on that electrode. At the outer boundaries, $\partial\phi/\partial n = 0$ is assumed.

Next we consider the electric potential due to the net charge in the plasma, equation (8). The net charge density within the plasma at any point is[24]:

$$\rho_c/\varepsilon_o = e(n_i - n_e)/\varepsilon_o \approx -\frac{en_o}{\varepsilon_o}\left[\exp\left(e\varphi/kT_i\right) + \exp\left(e\varphi/kT_e\right)\right] \tag{14}$$

where, e is elementary charge; n_i and n_e are the ion and electron densities in the plasma; n_o is the background plasma density; k is the Boltzmann's constant; T is the temperature of the species; and φ is the local electric potential. Expanding the exponential functions in a Taylor series for $\varphi \ll T$, equation (14) becomes, to lowest order of φ/T;

$$\rho_c/\varepsilon_o = -(e^2 n_o/\varepsilon_o)\left[\left(1/kT_i\right) + \left(1/kT_e\right)\right]\varphi. \tag{15}$$

Introducing the Debye length, λ_d,

$$\left(1/\lambda_d^2\right) = (e^2 n_o/\varepsilon_o)\left[\left(1/kT_i\right) + \left(1/kT_e\right)\right], \tag{16}$$

equation (15) becomes;

$$\rho_c/\varepsilon_o = \left(-1/\lambda_d^2\right)\varphi \tag{17}$$

And, alternatively, the electric potential is:

$$\varphi = \left(-\rho_c \lambda_d^2/\varepsilon_o\right). \tag{18}$$

Substituting (18) in Equation (8) we obtain an equation in terms of the net charge density at any point within the plasma.

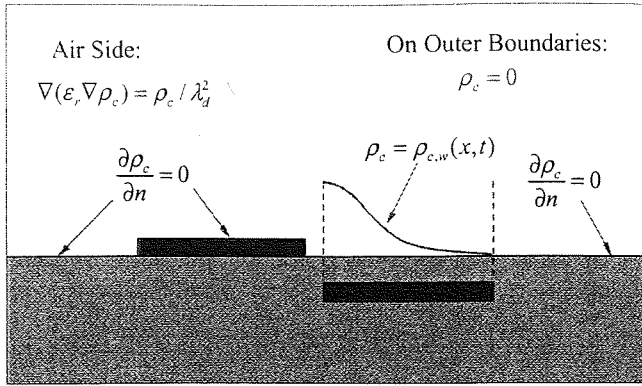$$\nabla \cdot (\varepsilon_r \nabla \rho_c) = \rho_c/\lambda_d^2. \tag{19}$$

Figure 4. Computational domain and boundary conditions for Equation 19.

Equation (19) is solved for the net charge density, ρ_c, only on the air side of the domain using the boundary conditions shown in Figure 4. A zero normal gradient for the net charge density is imposed on the solid walls except the region covering the lower electrode and the charge density is set to zero on the outer boundaries. Downstream of the exposed electrode, on the region over the embedded electrode the charge density is prescribed in such a way that it is synchronized with the time variation of the applied voltage $\phi(t)$ on the exposed electrode, $f(t)$ in equation (12):

$$\rho_{c,w}(x,t) = \rho_c^{max} G(x) f(t) \tag{20}$$

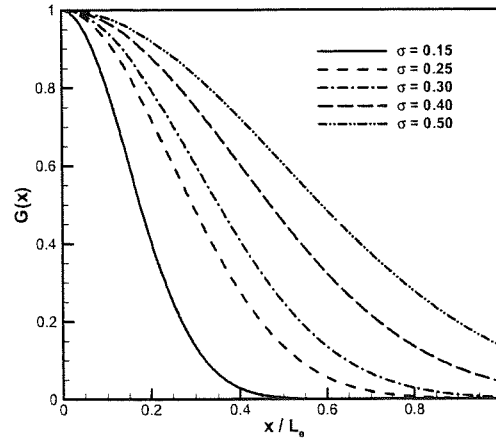where ρ_c^{max} is the maximum value of the charge density allowed in the domain (in Coulomb/m^3), a parameter to be determined later. The variation of the charge density on the wall, $\rho_{c,w}$, in the streamwise direction, x, is prescribed by a function $G(x)$ which can be chosen to resemble the plasma distribution over the embedded electrode. Experimental results[24,27,28] suggest that this distribution is similar to a half Gaussian distribution given by

$$G(x) = \exp\left[-(x-\mu)^2/(2\sigma^2)\right] \tag{21}$$

for $x \geq 0$. In equation (21) μ is the location parameter indicating the x location of the maximum, and σ is a scale parameter determining the rate of decay. Choosing a very large σ value results in a constant $\rho_{c,w}$ distribution. The variation of $G(x)$ with various values of σ defined in terms of the length of the electrode, L_e, is illustrated in figure 5. In this figure μ is equal to zero, and as σ increases the decay rate decreases.

In order to solve Eqs. (7) and (19), the Debye length, λ_d, maximum charge density on the wall, ρ_c^{max}, scale parameter for charge density distribution, σ, have to be prescribed. These parameters can be calibrated based on a simple experiment having a pure plasma-driven flow in a quiescent environment, as will be explained in the next section. In the computations we have chosen the location parameter μ such that the peak corresponds to the left edge of the embedded electrode as shown in Figure 4. Moreover, we have assumed that σ takes a value of 0.3 to allow a gradual decay of the charge density distribution from the left edge to the right edge. The values of the frequency and amplitude of the applied voltage, ω and ϕ^{max} in equations (12), (13a) and (13b) are given from the experiments.

Figure 5. Half Gaussian distribution given by Equation (21)

Once ϕ and ρ_c are obtained from solutions of equations (7) and (19) respectively, the resulting body force vector is computed from Equation (1), that is:

$$\vec{f}_B = \rho_c \vec{E} = \rho_c(-\nabla\phi). \tag{22}$$

It must be noted that solution of equations (7) and (19) is done only once at the beginning of computations, since these equations do not contain a time derivative term. This can be achieved by normalizing ϕ using the value of AC

voltage of the exposed electrode, $\phi(t)$, in equation (12). Equation (7) can then be solved by imposing a constant boundary condition equal to unity at the upper electrode. Once the dimensionless ϕ distribution is determined, the dimensional ϕ values at any given time can be obtained by multiplying this distribution with the corresponding value of $\phi(t)$ given by equation (12). Similarly, equation (19) can be solved at the beginning of computations by solving the dimensionless charge density distribution, which is normalized by $\rho_c^{max} f(t)$. This implies that the boundary condition for the dimensionless charge density on the wall region covering the embedded electrode is $G(x)$. Once the solution for the dimensionless charge density is established, the dimensional values at any time can be calculated from this distribution by multiplying it with the corresponding value of $\rho_c^{max} f(t)$.

This modeling approach for plasma actuators is implemented in the GHOST code developed at University of Kentucky. GHOST is a pressure-based code based on SIMPLE algorithm with second order accuracy in both time and space. Advection terms are approximated by a QUICK scheme and central differencing is used for the viscous terms. The 'Rhie and Chow' momentum interpolation method[29] is employed to avoid checkerboard oscillations usually associated with the non-staggered grid arrangement. This code is capable of handling complex geometries, moving and overset grids, and includes multiprocessor computation capability using MPI. Since multiple processors are used during the computations, it is more efficient to divide the computational domain into several smaller pieces with very fine grids and distribute the zones to processors with the consideration of equaling load balancing. The overset grid capability of the code enables incorporation of plasma actuators into the computations with relative ease since electrodes can be defined as individual solid blocks. The domain can be divided into two separate computational domains: one for the air side and the other for the dielectric wall. The GHOST code has been previously validated against a wide range of test cases and flow conditions and has been used extensively in several low pressure turbine related publications.[30-33]

III.   Results and Discussion

A. Model Validation and Calibration using Quiescent Flow Experiments

In order to calibrate the parameters Debye length, λ_d and the maximum charge density on the wall, ρ_c^{max}, appearing in the model we have chosen the quiescent flow experiments (Ref 34) conducted using a single pair of electrodes to better isolate the effects of the actuator on the surrounding air. The details of the actuator geometry and experimental set up are shown in Figure 6. The actuator consists of two 1cm wide conductive copper strips as electrodes which are separated by Kapton dielectric with ε_r value of 2.7.

$$t_e = 0.102 \text{ mm} \qquad x_e = 0.5 \text{ mm}$$
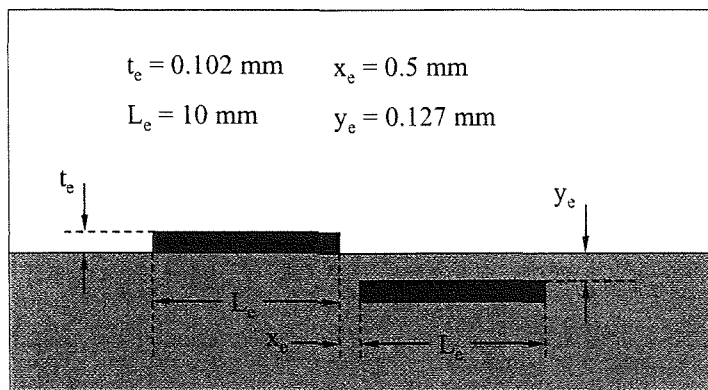$$L_e = 10 \text{ mm} \qquad y_e = 0.127 \text{ mm}$$

Figure 6. Experimental set up and details of the plasma actuator.

In the experiments the lower electrode is grounded and plasma region is generated using a square wave with frequency of, $\omega = 4.5 \text{ kHz}$ and amplitude of $\phi^{max} = 5 \text{ kV}$. The experimental data include velocity field measurements obtained using multiple PIV systems. Further details of the experiments and the measurement techniques used are given in Ref. 34. It should be noted that the experimental data are not intended to be used to calibrate the model and the experimental errors have not been quantified. Therefore, we shall only use these data for purpose of demonstration and a more comprehensive refinement of the model will follow in future work.

In the computations our aim is to match the maximum velocity observed in the experiments as well as the experimentally observed flow pattern shown in Figure 7a. From the experiment it is observed that the flow is drawn into the surface region above the embedded electrode by the plasma induced body force. This results in a jet issuing to the right of the actuator with a maximum velocity of approximately 1 m/s.
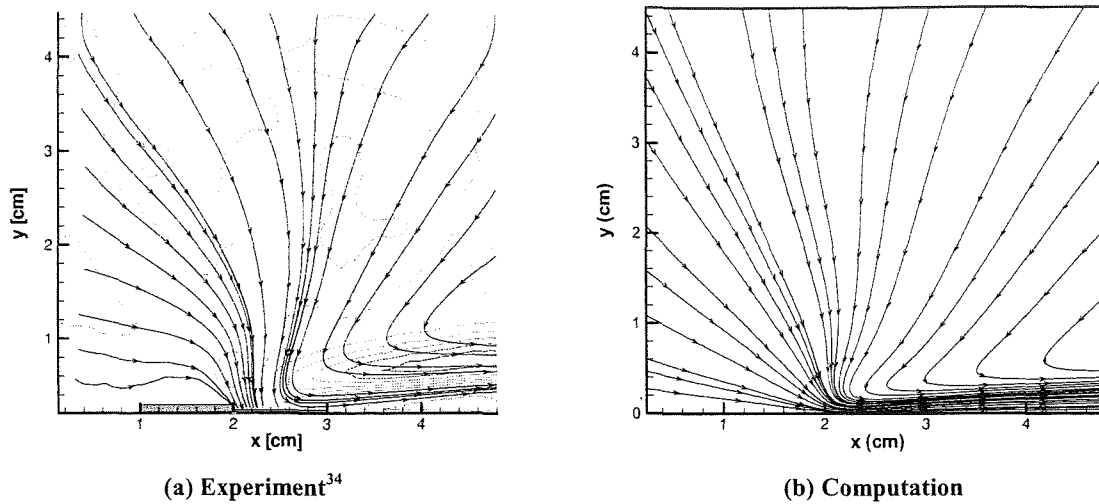

(a) Experiment[34]   (b) Computation

Figure 7. Comparison of experimental[34] and computed streamlines for the plasma actuator in quiescent flow. The actuator interface is located at the 2cm tick.

Based on the flow pattern and maximum velocity criteria, a choice of the parameter values of λ_d =0.001m and ρ_c^{max} =0.0008C/m^3 seems to agree well with the experiment. The streamlines obtained from the computation using these values are shown in Figure (7b). Although not an exact match, the computed flow pattern compares favorably with the experimental flowfield shown in Figure (7a). The computed maximum velocity is 1m/s also matching the experimental value. It should be noted that the boundary layer obtained by the computation appears to be thinner than the experimental data. Although the thickness can be adjusted by increasing the value of the Debye length, λ_d, we did not attempt to do so because the experimental data may be contaminated by 3-D effects caused by the experimental setup. A refinement of the model will be performed when more accurate data are available.

The computed electric potential distribution in the vicinity of the electrodes obtained from equation (7) is shown in Figure 8 along with the streamlines of the actuator induced flow. The computed electric potentials show that the strongest electric potential variation, or the electric field, is in the region between the two electrodes. This is also the region where the strongest concentration of plasma is observed in the experiments. The streamlines indicate that the flow is pulled from above into this region and jetted to the right direction.
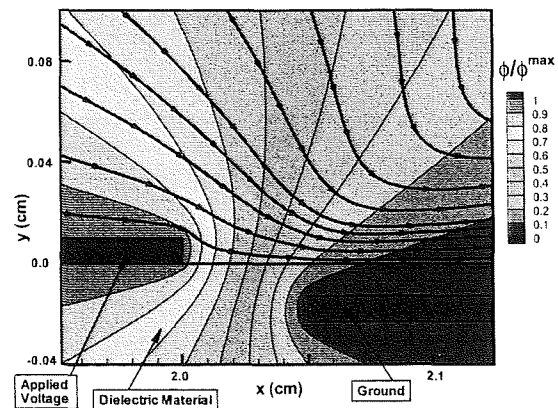

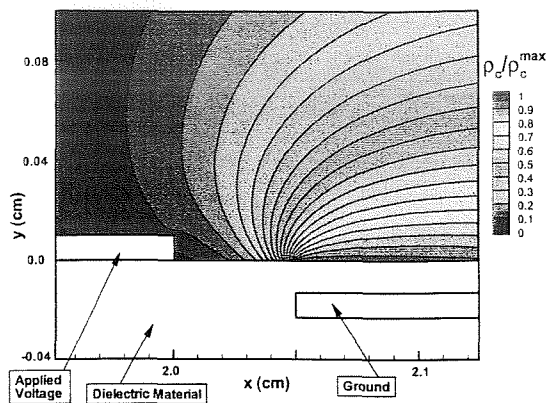**Figure 8. Computed electric potential contours and streamlines in the vicinity of the electrodes.**

Figure 9. Computed charge density contours in the vicinity of the electrodes.

Figure 10. Computed body force magnitude contours in the vicinity of the electrodes.

The charge density distribution obtained from equation (19) is shown in Figure 9. The charge density has its maximum value in the region over the corner of the embedded electrode as specified by the half Gaussian distribution. A thin layer of plasma is formed on the surface above the embedded electrode and gradually creeps into the gap staggered between the two electrodes as shown in Figure 9. This predicted charge density distribution resembles the plasma profile observed in the experiments.

The contours of magnitude of the computed body force vectors are shown in Figure 10. The highest body force is concentrated in the region over the upper left corner of the embedded electrode, where the concentration of charge density and the electric field strength are at maximum, consistent with the location where the strongest plasma generation is observed experimentally.
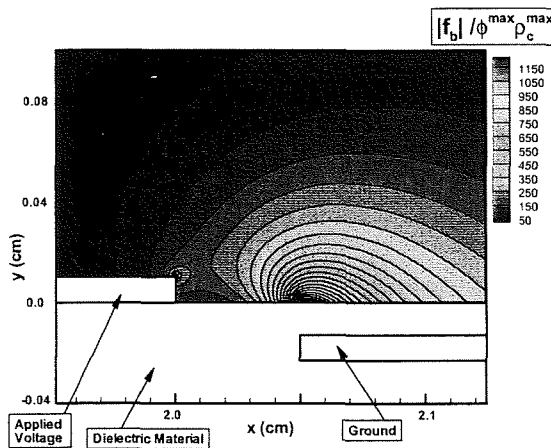
These results indicate that the model can mimic the experimentally observed effects caused by plasma actuators. It must be noted that, in this study we have limited the calibration of the model to a single experiment in order to provide a proof of concept for the model and the modeling approach. The results illustrate that the model and the approach are promising in the computation of plasma flow control applications. However, the model has to be further tested and the model parameters need to be further calibrated using more reliable experimental data.

B. Flow Separation Control in a Low Pressure Turbine Cascade

In order to illustrate the models applicability to plasma flow control applications a test case involving a low pressure turbine cascade is computed. We have selected an intermediate Reynolds number case from the Pratt and Whitney Pak-B blade experiments of Huang et al.[9] . We chose this case for demonstration purposes because it has a large flow separation region and the experimental data taken includes velocity profiles at various stations on the suction side of the blade and the pressure coefficient distribution. Further comparisons are available in Jacob et al.[16] The flow conditions are Re= 50,000 based on cascade inlet velocity and axial chord length and the freestream turbulence intensity is 0.08%. The experimental data for the base flow without flow control was used in this study. The flow separation zone is characterized by the plateau in the Cp distribution on the suction side of the blade. It is observed experimentally that the separation for the no-actuator flow extends from $x/C_x \approx 0.7$ to 0.95, as shown in Figure 11. Figure 11 also shows the comparison of the C_p distribution on the surface of the blade from the computation. The results show the separation starts at $x/C_x \approx 0.7$ but ends slightly earlier than the experimental location.
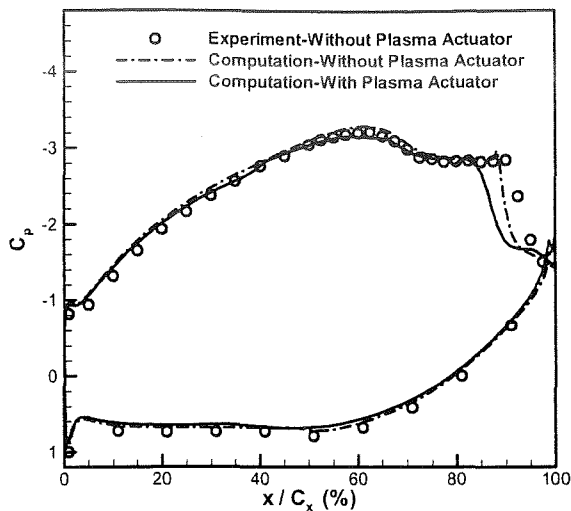
**Figure 11. Comparison of pressure coefficient distribution for Pak-B Blade, Re=50,000, FSTI=0.08%.**

The same actuator configuration as discussed in section IIIA is introduced on the suction surface of the blade with actuator interface located at 65% axial chord. Note that the actuator that was used in the simulation is not identical to the actuator used in Huang et al.[9] A sine wave voltage with a frequency of 5kHz, and an amplitude of 5kV is applied in the current demonstration. As can be seen from Figure 11, the use of the plasma actuator has caused the separation to reduce in size. The comparison of velocity profiles at various stations on the suction surface of the blade is shown in Figure 12. The figure shows that the size of the separation is reduced to end at $x/C_x \approx 0.87$. Comparisons with experimental data of the same geometry using a plasma actuator show similar results, in that separation is not completely eliminated and an inflection point is still present, but losses are significantly reduced downstream of the actuator location.[16] The ability of the model to simulate a control of flow separation for a low pressure turbine blade is thus demonstrated.

IV.   Concluding Remarks

The current paper presents a new modeling approach to simulate flow control using plasma actuators. The model solves two additional equations representing electrical field and charge density of the ionized air. These two equations need to be solved only once before the computation. A body force vector can be deduced from the solutions of these two quantities and it can then be incorporated into Navier-Stokes equations to account for the plasma-actuator effects. The model is calibrated against a simple plasma-actuator-driven flow in a quiescent environment. The model is then used to simulate an actual low-pressure turbine flow to achieve reduction of flow separation.

Acknowledgments
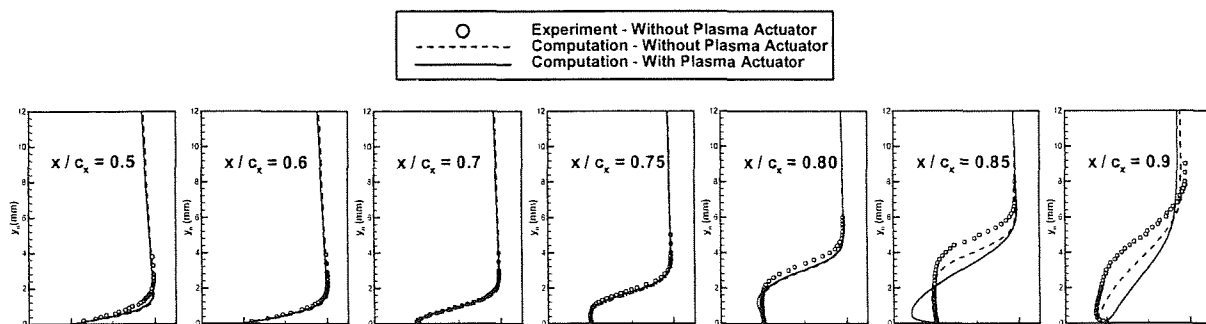
References

[1] Gad-el-hak, M.,1990, "Control of Low-Speed Airfoil Aerodynamics," AIAA Journal, Vol. 28., No. 9, pp. 1537-1552.

[2] Gad-el-hak, M.,2000, *Flow Control: passive, active, and reactive flow management*, Cambridge University Press.

[3] Gad-el-hak, M., Bushnell, D.M., 1991, "Separation Control: Review," Journal of Fluids Engineering, Vol. 113, pp. 5-30.

[4] Lord, W.K., MacMartin, D.G., Tillman, T.G., 2000, "Flow Control Opportunities in Gas Turbine Engines," AIAA-2000-2234.

[5] Rivir, R., Sondergaard, R., Bons, J.P., Lake, J.P., 2000, "Passive and Active Control of Separation in Gas Turbines," AIAA 2000-2235.

[6] Culley, D.E., Bright, M.M., Prahst, P.S., Strazisar, A.J., 2003, "Active Flow Separation Control of a Stator Vane Using Surface Injection in a Multistage Compressor Experiment," ASME-GT2003-38863.

[7] Bons, J., Sondergaard, R., Rivir, R., 1999, "Control of Low-Pressure Turbine Separation Using Vortex Generator Jets," AIAA-99-0367.

[8] Bons, J., Sondergaard, R., Rivir, R., 2001, "Turbine Separation Control Using Pulsed Vortex Generator Jets," Journal of Turbomachinery, Vol. 123.

[9] Huang, J., Corke, T.C., Thomas, F.O., 2003, "Plasma Actuators for Separation Control of Low Pressure Turbine Blades,"AIAA-2003-1027, AIAA 41st Aerospace Sciences Meeting and Exhibit, Reno, NV, January 2003.

[10] Roth, J.R., Sherman, D.M., Wilkinson, S.R., 2000, "Electrohydrodynamic Flow Control with a Glow-Discharge Surface Plasma,"AIAA Journal, Vol. 38, No. 7, July 2000.

[11] Corke, T., Cavalieri, D., Matlis, E., 2001, "Boundary Layer Instability on a Sharp Cone at Mach 3.5 with Controlled Input," AIAA Journal, Vol. 40, No 5., pp. 1015.

[12] Corke, T., Jumper, E., Post, M., Orlov, D., McLaughlin, T., 2002, "Application of Weakly ionized Plasmas as Wing Flow Control Devices," AIAA-2002-0350.

[13] Post, M.L., Corke, T., 2003, "Separation Control on High Angle of Attack Airfoil Using Plasma Actuators," AIAA 2003-1024.

[14] Orlov, D., Corke, T., Post, M., 2002, "DNS Modeling of Plasma Array Flow Actuators," Bulletin of the American Physical Society Fluid Dynamics Division, Annual Meeting.

[15] Hultgren, L.S., Ashpis, D.E., 2003, "Demonstration of Separation Delay with Glow-Discharge Plasma Actuators," AIAA-2003-1025. Reno, NV, Jan. 2003.

[16] Jacob, J., Rivir, R., Campbell, C., Estevedoreal, J., 2004, "Boundary Layer Flow Control Using AC Discharge Plasma Actuators." AIAA-2004-2128, 2nd Flow Control Conference, Portland, OR.

[17] Post, M.L., Corke, T., 2004, "Separation Control Using Plasma Actuators- Stationary & Oscillating Airfoils," AIAA-2004-0841.

[18] Morris, S.C., Corke, T.C., VanNess, D., Stephens, J., Douville, T., "Tip Clearance Control Using Plasma Actuators,", AIAA-2005-0782, January 2005.

[19] Shyy, W. Jayaraman, B., Andersson, A., "Modeling of Glow Discharge-Induced Fluid Dynamics," Journal of Applied Physics, Vol. 92, No. 11, pp. 6434-6443, December 2002.

[20] Hall, K.D., Jumper, E.J., Corke, T.C., McLaughlin, T.E., "Potential Flow Model of a Plasma Actuator as a Lift Enhancement Device," AIAA-2005-0783, January 2005.

[21] Orlov, D.M., Corke, T.C., "Numerical Simulation of Aerodynamic Plasma Actuator Effects," AIAA 2005-1083.

[22] Roy, S., Gaitonde, D., "Radio Frequency Induced Ionized Collisional Flow Model for Application at Atmospheric Pressures,", Journal of Applied Physics, Vol. 96, No. 5, pp. 2476-2481, September 2004.

[23] Roy, S., Gaitonde, D., "Modeling Surface Discharge Effects of Atmospheric RF on Gas Flow Control," AIAA-20050160, January 2005.

[24] Enloe, C.L., McLaughlin, T.E., VanDyken, R.D., Kachner, K.D., Jumper, E.J., Corke, T.C., Post, M., Haddad, O., 2004, "Mechanisms and Responses of a Single Dielectric Barrier Plasma Actuator: Geometric Effects," AIAA Journal, Vol. 42, No. 3, pp. 595-604, March 2004.

[25] Leonov, S., Bityurin, SV., Avischenko, N., Yuriev, A., and Gromov. V. 2001, "Influence of Surface Electrical Discharge on Friction of Plate in Subsonic and Transonic Airfoil." AIAA 39th Aerospace Sciences Meeting & Exhibit, AIAA, 2001, Paper 2001-0640.

[26] Patankar, N. A., Hu, H.H., "Numerical Simulation of Electroosmotic Flow," Analytical Chemistry, Vol. 70, No. 9, pp. 1870-1881, May, 1998.

[27] Enloe, C.L., Mclaughlin, T.E., Font, G.I., Baughn, J.W., "Parameterization of Temporal Structure in a Single Dielectric Barrier Aerodynamic Plasma Actuator," AIAA-2005-0564, January 2005.

[28] Enloe, C.L., Mclaughlin, T.E., VanDyken, R.D., Fischer, J.C., "Plasma Structure in the Aerodynamic Plasma Actuator," AIAA-200-0844, January 2004.

[29] Rhie, C. M. and Chow, W. L. 1983, "Numerical study of the turbulent flow past an airfoil with trailing edge separation," AIAA Journal Vol.21, pp.1525-1532.

[30] Suzen, Y.B., Huang, P.G., "Numerical Simulation of Unsteady Wake/Blade Interactions in Low Pressure Turbine Flows Using an Intermittency Transport Equation," ASME-GT2004-53630, ASME Turbo-Expo 2004, Vienna, Austria, June 2004.

[31] Suzen, Y.B., Huang, P.G., "Numerical Simulations of Transitional Flows as Affected by Passing Wakes," AIAA-2004-0103, 42nd Aerospace Sciences Meeting and Exhibit, Reno, NV, January 2004.

[32] Suzen, Y.B., Huang, P.G., "Comprehensive Validation of an Intermittency Transport Model for Transitional Low-Pressure Turbine Flows," AIAA-2004-1121, 42nd Aerospace Sciences Meeting and Exhibit, Reno, NV, January 2004.

[33] Suzen, Y.B., Huang, P.G., Volino, R.J., Corke, T.C., Thomas, F.O., Huang, J., Lake, J.P., King, P.I., "A Comprehensive CFD Study of Transitional Flows in Low-Pressure Turbines Under a Wide Range of Operating Conditions", AIAA-2003-3591, 33rd AIAA Fluid Dynamics Conference, Orlando, FL, June 2003.

[34] Jacob, J.D., Ramakumar, K., Anthony, R., Rivir, R.B., "Control of Laminar and Turbulent Shear Flows Using Plasma Actuators," To be published in Fourth International Symposium on Turbulence and Shear Flow Phenomena, TSFP-4, Williamsburg, VA, June 2005.